DOI: 10.3969/j.issn.1673-3185.2017.03.010 **http:** // english.ship-research.com

Translated from: XU W Z, WU W G. Development of in-house high-resolution hydrocode for assessment of blast waves and its application[J]. Chinese Journal of Ship Research, 2017, 12(3): 64-74.

Development of in-house high-resolution hydrocode for assessment of blast waves and its application

XU Weizheng[1,2], *WU Weiguo*[1,2]

1 Key Laboratory of High Performance Ship Technology of Ministry of Education, Wuhan University of Technology, Wuhan 430063, China

2 School of Transportation, Wuhan University of Technology, Wuhan 430063, China

Abstract: The propagation and evolution characteristics of blast waves in confined spaces are complicated due to the constraint of the surrounding walls, by which the enhanced reflected shock waves will cause more serious damage to the internal structures, facilities and personnel. In order to investigate the characteristics of explosions in confined spaces, an in-house high-resolution hydrocode was developed in this present work. The third-order WENO finite difference scheme (weighted essentially non-oscillation scheme) was implemented in the code to capture the shock waves generated by cylindrical explosives. The Sod shock tube problem, interacting blast wave problem and blast in air problem were simulated to validate the code. The validated code was then used to simulate the blast waves generated by condensed explosives in closed, vented and connected spaces. The propagation of blast waves and the characteristics of blast load were subsequently investigated. The developed code appears to accurately predict the process of explosions in confined spaces. This high-resolution hydrocode can be used to study the propagation paths of blast waves in complicated spaces and evaluate the internal blast load, which can provide reliable input for the design of explosion-resistant structures.

Key words: explosive shock wave; confined space; numerical simulation; high-resolution hydrocode; WENO scheme; program development

CLC number: U661.4

0 Introduction

With the rapid development of modern anti-ship weapons, all kinds of semi-armor-piercing anti-ship missiles with high-performance have become the main threat to the side above waterline of surface ship. The feature of the damage to the ship is that the missile penetrates the planking of ship side and causes the explosion in the cabin. When the explosion happens in the cabin, as the shock waves are constrained by the surrounding walls in the process of propagation, the shock waves with short duration and gradually decreasing peak as well as quasi-static overpressure with long duration [1-2] will be generated and cause serious damage to the cabin structure, internal facilities and personnel. In recent years, scholars at home and abroad have carried out a lot of research on blast load in the cabin and confined spaces from the aspects of test, numerical simulation and high-resolution numerical method.

Edri et al. [3] carried out TNT explosive experiments in a cuboid room with venting holes and analyzed the influence law of charge quality on the internal blast load. Wu et al. [4] carried out explosive ex-

Received: 2016-11-28

Supported by: Foundation of National Ministries and Commissions; National Natural Science Foundation of China (51409202)

Author(s): XU Weizheng, male, born in 1991, Ph.D. candidate. Research direction: high-precision numerical calculation and 3D program development of blast waves. E-mail: xuweizheng@whut.edu.cn

WU Weiguo(Corresponding author), male, born in 1960, professor, doctoral supervisor. Research direction: structural dynamics. E-mail: mailjt@163.com

periments in closed space and studied the influence law of explosive shape and detonation location on explosive shock waves. Hu et al. [5] recorded the pressure time history curve of blast load on the walls in confined space of cuboid concrete with a pressure sensor, and analyzed the distribution law of the blast load on the walls. Hou et al. [6] carried out the research on the load characteristics of the explosive shock waves in the cabin. Kong et al. [7] studied the influence law of corner structures on the blast load in the cabin. Hou et al. [8] studied the load characteristics of the explosive shock waves in the cabin based on MSC.DYTRAN software. KONG et al. [9] studied the explosion and its damage effect of warhead in the ship cabin based on MSC.DYTRAN software. Ding et al. [10] simulated the in-house blast by Remap technology of AUTODYN commercial software and studied the distribution of blast load on the walls. Fan et al. [11] carried out the numerical simulation on the propagation characteristics of blast load in the large and typical cabin with complex structure by using LS-DYNA software.

To sum up, the current research on blast load in the confined spaces is mainly carried out by two means, namely, experimental test and numerical simulation of commercial software. Considering the high cost and risks of the explosive test, numerical stimulation has become the main method to study the blast waves'propagation and blast load characteristics. However, the solver of current commercial softwares including LS-DYNA, MSC.DYTRAN and AUTODYN mainly adopts traditional second-order accuracy algorithm to simulate the blast process, such as Euler-FCT method of finite difference and Roe method of finite volume. Due to the low accuracy of calculation, these methods seriously smooth the peak pressure of explosive shock waves. The accurate prediction of blast load is the basis for proper design and evaluation of explosion-resistant structure. The current mature high-resolution method has not been integrated into the commercial softwares, so the study and development of high-resolution hydrocode for assessment of blast load are of great engineering significance.

For the explosion issue with high pressure ratio and high density ratio, higher requirements are put forward for shock wave capture schemes in the numerical simulation. In this paper, Liu et al. [12] proposed the weighted essentially non-oscillation scheme (WENO scheme) in 1994 and Shu et al. [13-15] developed this scheme. The WENO scheme performs better than ENO scheme [16] in effectivity, flux smoothness and stability of convergence solution. So using WENO scheme in simulating the blast process is a favorable choice.

Based on the FORTRAN platform and using the third-order WENO finite difference scheme, this paper aims to independently develop the high-resolution hydrocode for assessment of blast waves and study the blast waves'propagation law and blast load characteristics in the closed, venting and connected spaces by the high-resolution hydrocode. The research provides the reference for the later studies in the propagation of blast waves, blast load and the design of explosion-resistant structures.

1 Program development

1.1 Euler equation

Based on the assumption of instantaneous detonation, the explosive is equivalent to the gas with high pressure and high density. The governing equation of explosion field can be described by the three-dimensional compressible Euler equation [17] as follows:

$$\frac{\partial \boldsymbol{U}}{\partial t}+\frac{\partial \boldsymbol{E}}{\partial x}+\frac{\partial \boldsymbol{F}}{\partial y}+\frac{\partial \boldsymbol{G}}{\partial z}=0 \tag{1}$$

where $\boldsymbol{U}$ is the conservative flux; $\boldsymbol{E}$, $\boldsymbol{F}$ and $\boldsymbol{G}$ are the numerical fluxes. They are respectively shown by the following equations.

$$\boldsymbol{U}=\begin{pmatrix}\rho\\ \rho u\\ \rho v\\ \rho w\\ E\end{pmatrix},\quad \boldsymbol{E}=\begin{pmatrix}\rho u\\ \rho u^2+p\\ \rho uv\\ \rho uw\\ u(E+p)\end{pmatrix},$$

$$\boldsymbol{F}=\begin{pmatrix}\rho v\\ \rho vu\\ \rho v^2+p\\ \rho vw\\ v(E+p)\end{pmatrix},\quad \boldsymbol{G}=\begin{pmatrix}\rho w\\ \rho wu\\ \rho wv\\ \rho w^2+p\\ v(E+p)\end{pmatrix}$$

$$E=\rho e+\frac{1}{2}\rho u^2+\frac{1}{2}\rho v^2+\frac{1}{2}\rho w^2 \tag{3}$$

$$p=(\gamma-1)\rho e \tag{4}$$

where ρ is the density; u, v and w are the velocity components in the directions of x, y and z respectively; p is the fluid pressure; E is the total energy of the fluid per unit volume; e is the specific internal energy; γ is the adiabatic exponent of gas and is set to be 1.4 in this paper.

1.2 Numerical discretization method

By using the Strang dimensional split method, Eul-

er equation is decomposed into x, y and z directions for solving. The numerical discretization of Euler equation's space item is carried out by the third-order WENO finite difference scheme. The specific discretization process is as follows.

The numerical flux $f_{i+1/2}$ of the $x_{i+1/2}$ center point is:

$$f_{i+1/2}=\frac{1}{2}(f_i+f_{i+1})-\frac{1}{2}\omega_0(D_0-D_1) \quad (5)$$

where f_i and f_{i+1} are separately the numerical fluxes of the x_i and x_{i+1} points; ω_0 is the nonlinear weight; $D_0=f_{i-1}-f_i$; $D_1=f_i-f_{i+1}$.

ω_0 in Eq. (5) can be solved by the following equation:

$$\omega_0\frac{\alpha_0}{\sum_{s=0}^{1}\alpha_k}$$

$$\alpha_k=\frac{d_k}{(\varepsilon+\beta_k)};k=0,1$$

$$d_0=\frac{1}{3},\ d_1=\frac{2}{3} \quad (6)$$

where ε is the decimal to avoid the zero denominator, which is taken as 1.0×10^{-6}; k is the number of third-order WEND subtemplates; d_k is the linear weight of third-order WENO scheme; α_k is the transfer function. The two subtemplates of the third-order WENO are $\{x_{i-1},x_i\}$ and $\{x_i,x_{i+1}\}$; $\beta_k(k=0,1)$ is the smoothness factor and its equation is as follows [18]:

$$\begin{cases}\beta_k=D_0^2\\ \beta_1=D_1^2\end{cases} \quad (7)$$

The numerical discretization of Euler equation's time item is carried out by using the third-order TVD-RK method [19]. The specific discretization scheme is as follows:

$$\begin{cases}\boldsymbol{U}^{(1)}=\boldsymbol{U}^n+\Delta tL(\boldsymbol{U}^n)\\ \boldsymbol{U}^{(2)}=\frac{3}{4}\boldsymbol{U}^n+\frac{1}{4}\boldsymbol{U}^{(1)}+\frac{1}{4}\Delta tL(\boldsymbol{U}^{(1)})\\ \boldsymbol{U}^{n+1}=\frac{1}{3}\boldsymbol{U}^n+\frac{1}{3}\boldsymbol{U}^{(2)}+\frac{2}{3}\Delta tL(\boldsymbol{U}^{(2)})\end{cases} \quad (8)$$

where $\boldsymbol{U}^n$ is the conservative flux at moment n; and $\boldsymbol{U}^{(1)}$ and $\boldsymbol{U}^{(2)}$ are the intermediate variables; $\boldsymbol{U}^{n+1}$ is the conservative flux at moment $n+1$; Δt is the time step; and $L(\cdot)$ is operator.

2 Calculation examples for verification

2.1 Sod shock tube

The initial condition of this calculation example is shown in Eq. (9) [20]. The boundary condition is set as the outflow boundary. The number of meshes is 200 and the end time of calculation is 0.18. The dimensionless pressure curves at the end of the calculation are shown in Fig. 1.

$$(\rho,u,p)^{\mathrm{T}}=\begin{cases}(1,0,1)^{\mathrm{T}}, & 0\leqslant x<0.5\\ (0.125,0,0.1)^{\mathrm{T}}, & 0.5\leqslant x\leqslant 1\end{cases} \quad (9)$$

where ρ, u and p are respectively the dimensionless density, velocity and pressure.

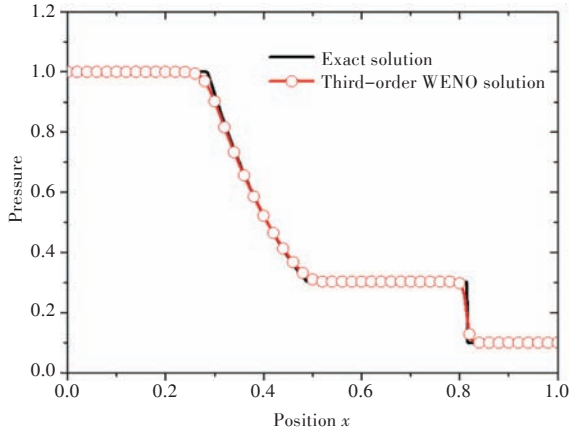

Fig.1 Pressure curves calculated by the case of the sod shock tube

2.2 Interacting blast wave

The initial condition of this calculation example is shown in Eq. (10) [21]. The boundary condition is set as the reflection boundary. The number of meshes is 800 and the end time of calculation is 0.038. The dimensionless pressure curves at the end of the interacting blast wave are shown in Fig. 2.

$$(\rho,u,p)^{\mathrm{T}}=\begin{cases}(1,0,1000)^{\mathrm{T}}, & 0\leqslant x<0.1\\ (1,0,0.01)^{\mathrm{T}}, & 0.1\leqslant x\leqslant 0.9\\ (1,0,100)^{\mathrm{T}}, & 0.9\leqslant x\leqslant 1\end{cases} \quad (10)$$

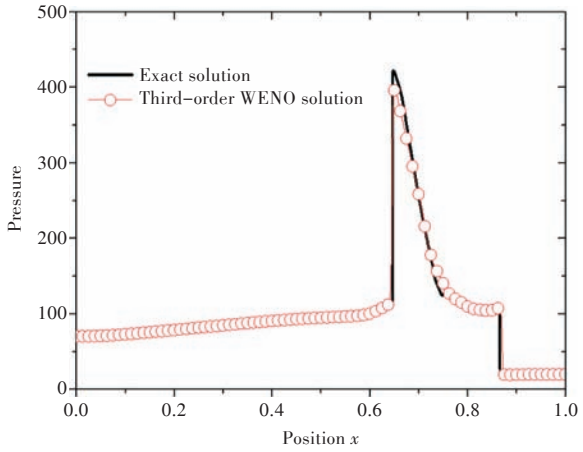

Fig. 2 Pressure curves calculated by the case of the interacting blast wave

2.3 Blast in air

The length of the computational domain is designed as 5,000 mm and the charge radius is 100

mm. The parameters of gas with high pressure and high density after the equivalence of instantaneous detonation are as follows: ρ = 1,630 kg/m^3, P = 3.057,9 × 10^9 Pa. Through a number of numerical tests, the mesh size is set as 10 mm. Fig. 3 shows the comparison of the pressure time history at typical locations (namely, 2 m and 3 m) and output results of AUTODYN commercial program.

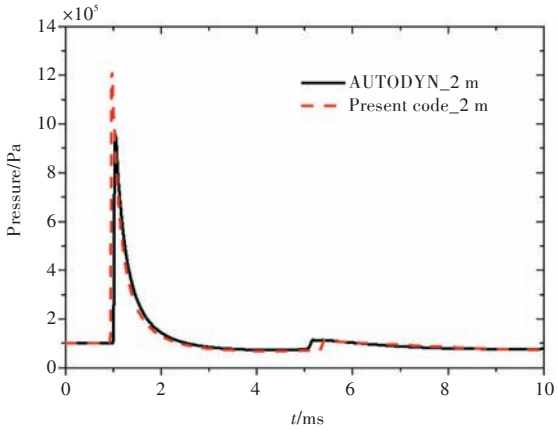

(a) At typical location of 2 m

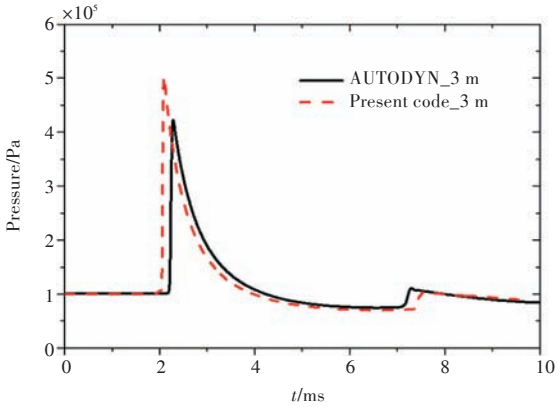

(b) At typical location of 3 m

Fig.3 Comparisons of pressure time history of blast in air at typical locations

From the comparison results in Fig. 1, Fig. 2 and Fig. 3, it can be seen that the numerical calculation program developed in this paper has high accuracy and certain reliability.

3 Blast in closed space

3.1 Setting of initial condition

The size of the closed space is set as 1,800 mm × 800 mm × 800 mm. There are five measuring points (No. 1–No. 5) on the walls for outputting the explosion overpressure time histories (see Fig. 4). Cylindrical explosive of 500 g is placed at the center of the closed space. The parameters of the equivalent gas with high pressure and high density are as follows: radius is 99 mm, height is 80 mm, ρ =203.75 kg/m^3, P = 3.822 × 10^8 Pa. The initial conditions of calculation are shown in Fig. 5(a). Considering the requirements of calculation time and accuracy, the number of meshes is set as 0.144 million (90 × 40 × 40) after several numerical tests, as shown in Fig. 5(b). The boundary condition of the walls is set as the boundary condition of rigid reflection. The coupling effects of the shock waves and the structure are not taken into consideration here.

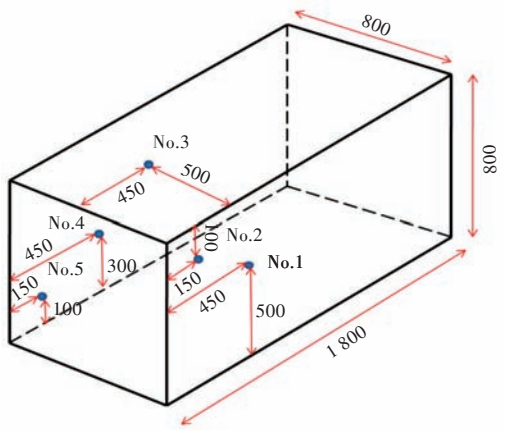

Fig.4 Schematic diagram of closed space and arrangement of measuring points

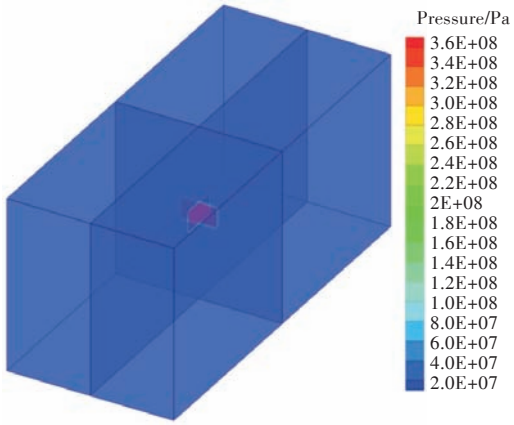

(a) Initial field of blast

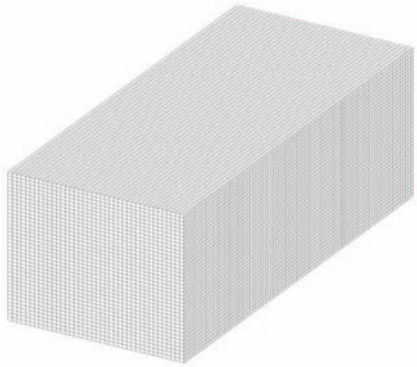

(b) Mesh distribution

Fig.5 Initial conditions and mesh distribution in closed space

3.2 Propagation process of blast wave

The pressure distribution of different moments at early stage of explosion in the closed space is shown

in Fig. 6. From Fig. 6, the propagation process of the blast waves in the early stage of the explosion can be analyzed. The high pressure gas first undergoes the three-dimensional cylindrically symmetric free expansion. The regular reflection occurs when the blast waves arrive at the walls for the first time (see Fig. 6 (a)). Due to the constraints of surrounding walls, the blast waves propagate toward the end face in the longitudinal direction of the closed space and form a local pressure convergence phenomenon at the intersection of two walls. The local convergence pressure peak propagates along the longitudinal direction of the closed space (see Fig. 6(b)). When the blast waves reach the end face of the closed space, the pressure convergence phenomenon occurs in the vicinity of the three-wall corner (see Fig. 6(c)). Then two sides of the reflected waves propagate towards the center of the closed space in the form of approximate plane wave (see Fig. 6(d)).

3.3 Blast load characteristics

Fig. 7 shows the time history curve of the overpressure and impulse (I) of measuring points on the explosion walls in the closed space at different moments. It can be seen from Fig. 7(a) that at early

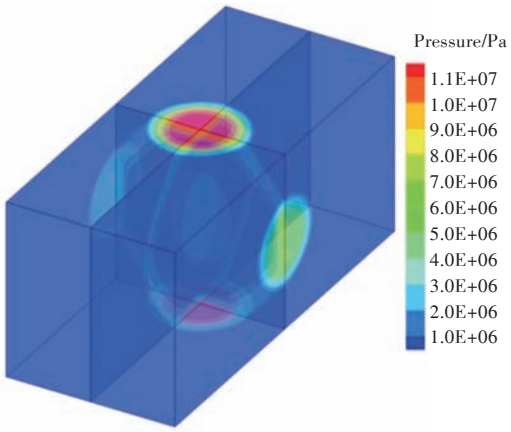

(a) t=0.137 9 ms

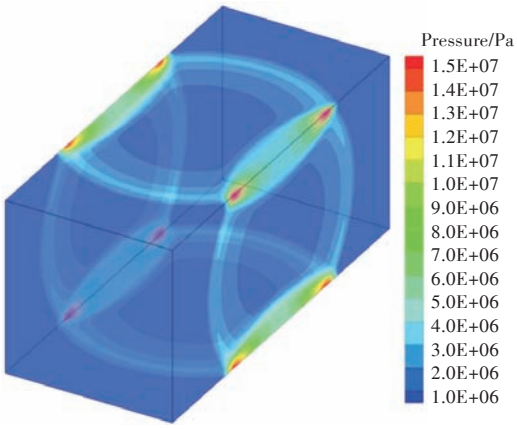

(b) t=0.325 6 ms

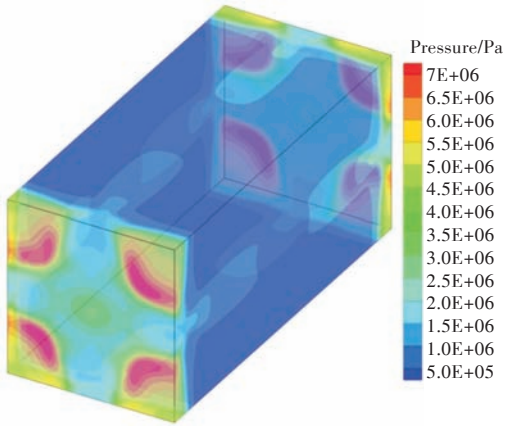

(c) t=0.701 2 ms

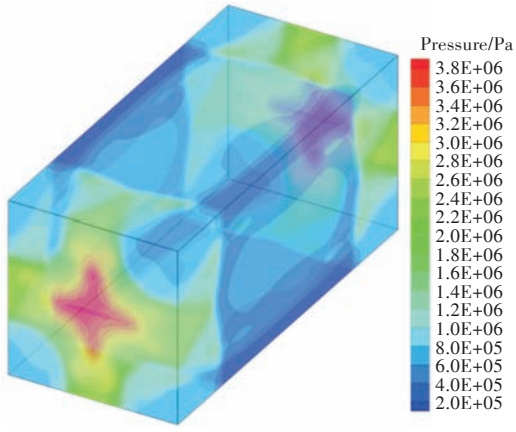

(d) t=0.930 5 ms

Fig.6 Pressure distribution at early stage in closed space

stage, the overpressure peaks of the blast waves at different measuring points are different (see Fig. 7 (a)) while the quasi-static overpressure peaks are almost the same (see the green heavy line in Fig. 7(a)), which indicates that the quasi-static overpressure peak formed by the explosion in the closed space is even spatially. As can be seen from Fig. 7(b), the time history curve of the measuring points on the explosion walls inside the confined space appears to be a straight line through the origin and the differences among the various measuring points are very small.

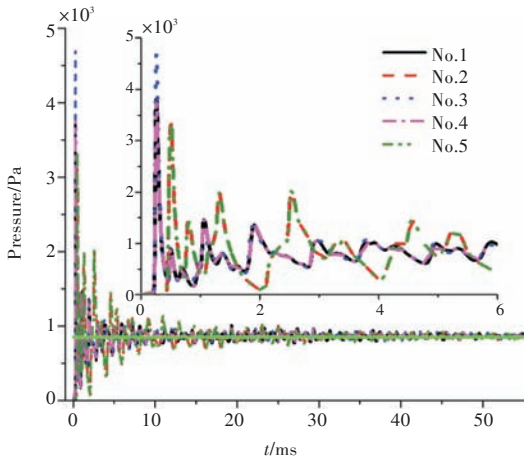

(a) Overpressure time history

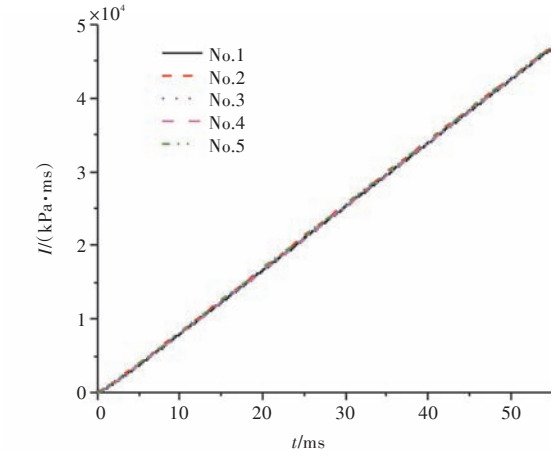

(b) Impulse time history

Fig.7 Time histories of blast load at the gauging points in closed space

4 Blast in venting space

4.1 Setting of initial conditions

The sizes and measuring points of the venting space are the same as those in Section 3.1 and the only difference is that there is a square venting hole on one wall in the longitudinal direction, as shown in Fig. 8. The length of the square venting hole is 320 mm which is taken as L320 mm in the following figures. Cylindrical explosive of 769 g is placed in the center of the venting space. The specific parameters of the equivalent gas with high pressure and high density are as follows: radius is 100 mm, height is 120 mm, ρ = 203.75 kg/m^3, p = 3.822 × 10^8 Pa. The initial conditions are shown in Fig. 9. Taking into account the requirements of the calculation time and accuracy, the number of meshes is still 0.144 million (90 × 40 × 40) after multiple numerical tests. The wall boundary condition is set as the boundary condition of rigid reflection and the boundary condition at the venting hole is set as the transmission boundary.

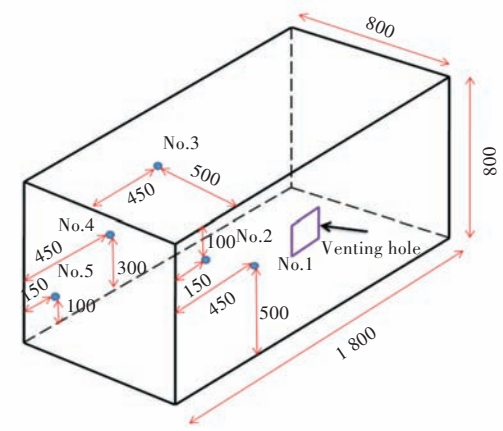

Fig.8 Schematic diagram of venting space and arrangement of measuring points

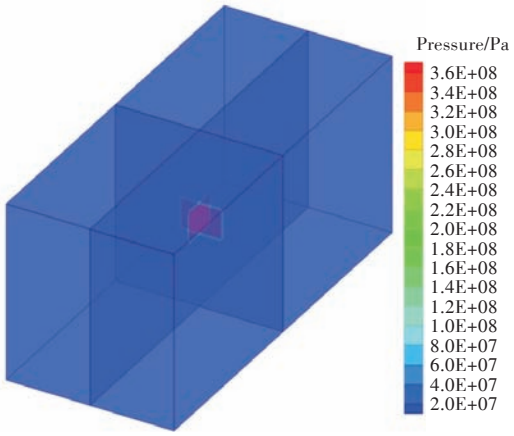

Fig.9 Initial conditions in venting space

4.2 Propagation process of blast wave

The pressure distribution of different moments at early stage of explosion in venting space is shown in Fig. 10. It can be known from Fig. 10 that the propagation process of blast wave in venting space basically follows the same law with that in closed space. The biggest difference is that as the high pressure gas vents from the venting hole, the pressure in the vicinity of the venting hole is reduced (Fig. 10(a)), but this venting process has little effect on the propagation process of high-intensity blast waves at early stage of the explosion.

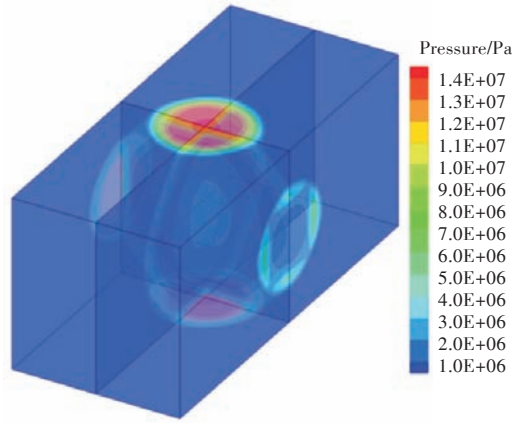

(a) t=0.136 2 ms

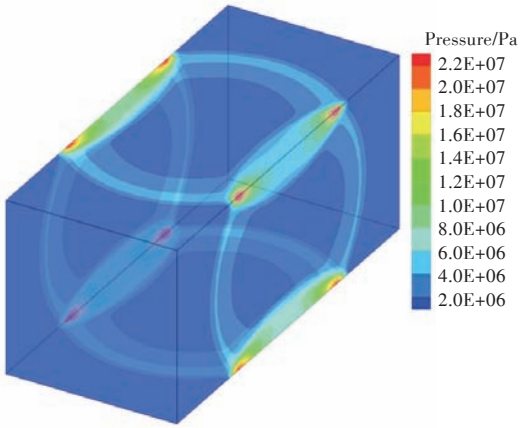

(b) t=0.302 9 ms

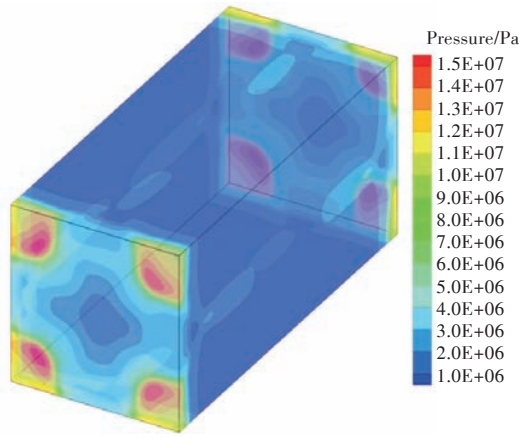

(c) t=0.592 5 ms

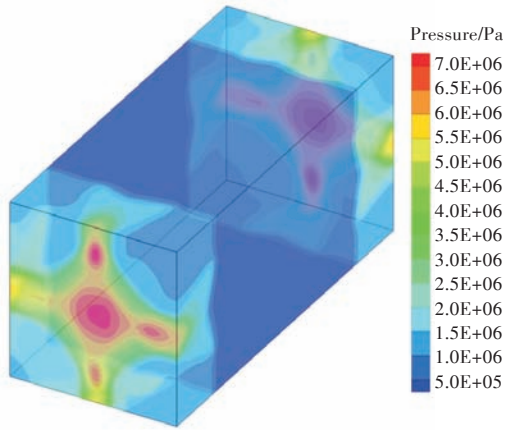

(d) t=0.793 8 ms

Fig.10 Pressure distribution at early stage in venting space

4.3 Blast load characteristics

Fig. 11 shows the time histories of overpressure and impulse (I) of the measuring points on the explosion walls in venting space. It can be seen from Fig. 11(a) that at early stage, the overpressure peaks of the blast waves at different measuring points are different, while the time histories of quasi-state overpressure are basically the same (see the green heavy line in Fig.11 (a)), which indicates that the quasi-static overpressure time history formed by the explosion in venting space is even spatially. The quasi-static overpressure curve follows the law of exponential decay, which is consistent with the assumptions based on a large number of experimental data in Ref. [22].

It can be seen from Fig. 11(b) that the impulse time history curve of the measuring points on the explosion walls in venting space appears to be a parabola through the origin and there are some differences for the various measuring points. Nos. 1, 3 and 4 measuring points are in the same tangent plane 1 (x = 1,350), of which the impulse time histories are basically the same; Nos. 2 and 5 are in the same tangent plane 2 (x = 1,650), of which the impulse time histories are basically the same. As the tangent plane 1 is closer to the venting hole compared with the tangent plane 2, the decay of the time histories in the tangent plane 1 tends to be faster.

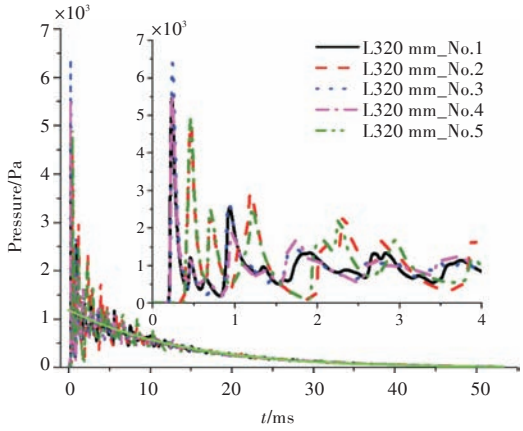

(a) Overpressure time history

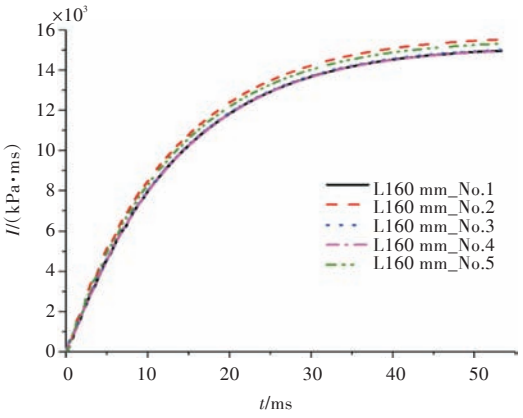

(b) Impulse time history

Fig.11 Time histories of blast load at the gauging points in venting space

4.4 Influence of venting hole location

This section mainly discusses the influence law of the venting hole location on the blast load in venting space. The sizes of the venting space are the same as those in Section 3.1, but three different venting hole locations are set as shown in Fig. 12: 450 mm to the left, the middle 0 mm and 450 mm to the right of the x direction of the half-length plane in the venting space. Fig. 13 shows the overpressure and impulse time histories at measuring point 3 at different venting hole locations.

It can be seen from Fig. 13 that the location of the venting hole has little effect on the quasi-static overpressure load in venting space, but exerts a certain effect on the impulse time histories. Shortening the relative distance between venting hole and the explosive can reduce the impulse.

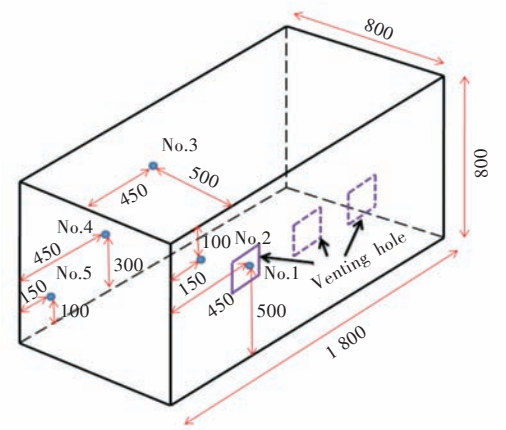

Fig.12 Schematic diagram of venting hole locations in venting space

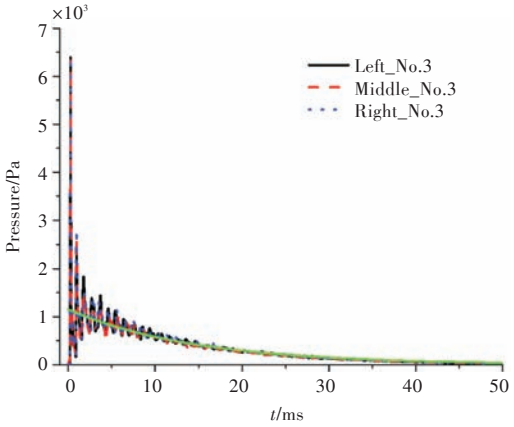

(a) Overpressure time history

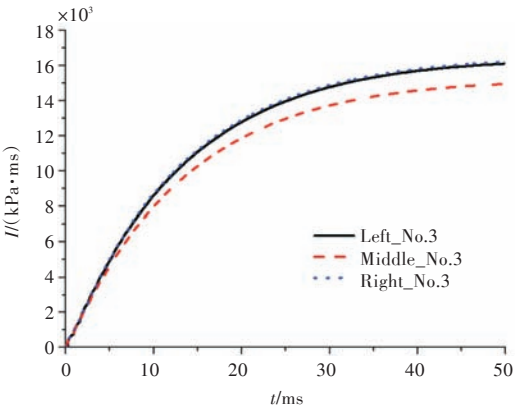

(b) Impulse time history

Fig.13 Time histories of blast load at gauging point 3 for different positions of venting hole

4.5 Influence of venting hole size

This section mainly discusses the influence law of venting hole size on the blast load in venting space. The sizes of the venting space are the same as those in Section 3.1, but three square venting holes with different lengths are set, namely, L80 mm, L160 mm and L320 mm. Fig. 14 shows the overpressure time histories at measuring point 3 for different venting hole sizes.

It can be seen from Fig. 14 that the sizes of the venting hole have significant influence on the quasi-static overpressure time history in venting space. The longer the side length of the venting hole is, the faster the decay of the quasi-static overpressure is (see Fig. 14(a)). Besides, the sizes of the venting hole have significant influence on the impulse time history as well. Increasing the size of the venting hole can significantly decrease the impulse (see Fig. 14(b)). It can be seen from the analysis that this is mainly because under the same blast wave intensity, the increasing length of the venting hole allows more energy to be vented from the hole in unit time.

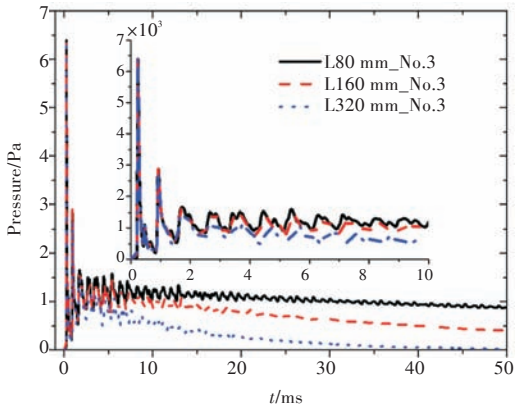

(a) Overpressure time history

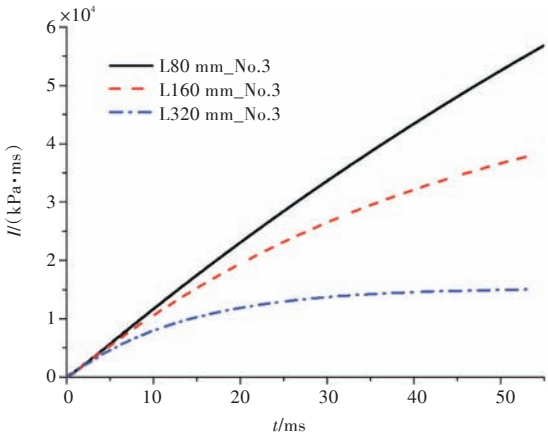

(b) Impulse time history

Fig.14 Time histories of blast load at point 3 for different sizes of venting holes

5 Blast in connected space

5.1 Setting of initial conditions

The connected space consists of two confined space with the same sizes and a square connecting tube in the middle of which the length of section is 400 mm. There are four measuring points (No.1–No.4) on the walls for outputting the overpressure time histories, as shown in Fig. 15. Cylindrical explosive of 769 g is placed inside the left confined

space. The specific parameters of the equivalent gas with high pressure and high density are the same as those in Section 4.1. The initial conditions of calculation are shown in Fig. 16(a). In the calculation process, the orthogonal regular meshes are taken. Considering the calculation time and accuracy and based on several numerical tests, the size of single mesh is set as 20 mm × 20 mm × 20 mm), as shown in Fig. 16 (b). The wall boundary condition is set as reflection boundary of rigid wall.

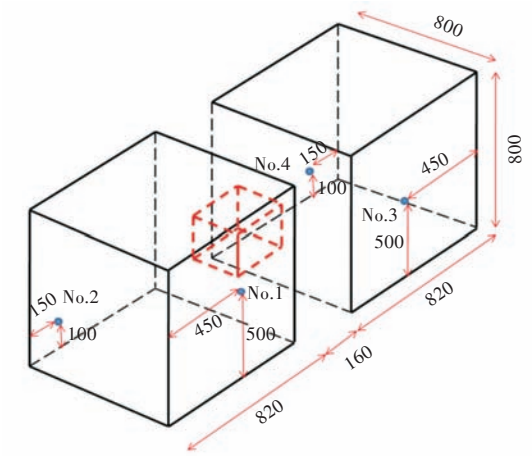

Fig.15 Schematic diagram of connected space and arrangement of measuring points

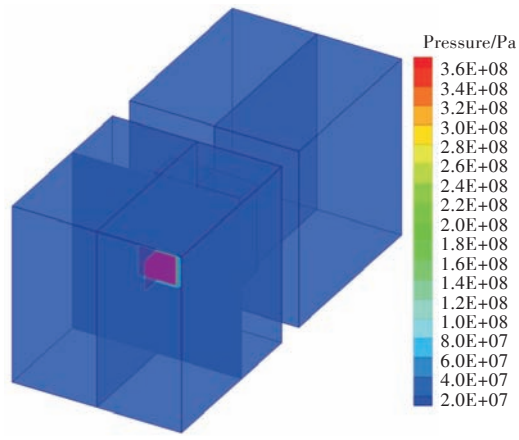

(a) Initial field of blast

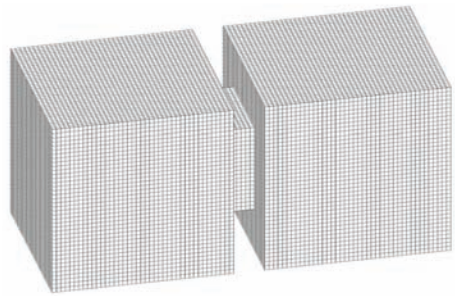

(b) Mesh distribution

Fig.16 Initial condition and mesh distribution in connected space

5.2 Propagation process of blast wave

Fig. 17 shows the pressure distribution at early stage in connected space. From Fig. 17, the propagation process of the blast waves in the early stage of the explosion can be analyzed. The high-pressure gas first carries out the three-dimensional cylindrically symmetric free expansion.

The regular reflection occurs when the blast waves reach the walls for the first time and some high-pressure gas vents from the venting hole to the right confined space, which makes the pressure in the vicinity of the venting tube lower (Fig. 17(a)). Due to the constraints of surrounding walls, the blast waves begin to form pressure convergence phenomenon in the vicinity of the left confined space corner (Fig. 17(b)). The blast waves propagate through the venting tube to the inside of the right confined space and propagate along the longitudinal direction (Fig. 17(c)). Then, the blast waves are reflected after arriving at the end face of the right confined space. The pressure convergence phenomenon is formed in the area near the corner of the right confined space. The pressure convergence phenomenon is formed in the corner of the left confined space due to the multiple reflections of the blast waves (Fig. 17(d)).

5.3 Blast load characteristics

Fig. 18 respectively shows the overpressure and impulse time histories of Nos. 1 and 2 measuring

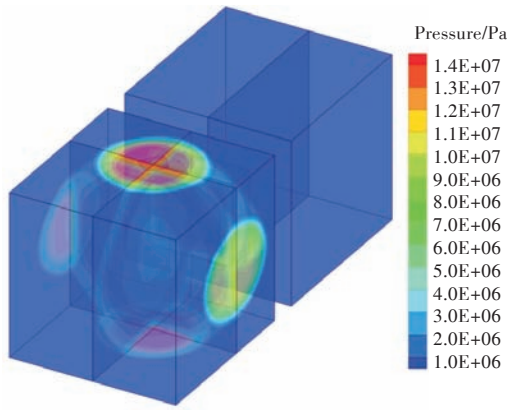

(a) t = 0.135 8 ms

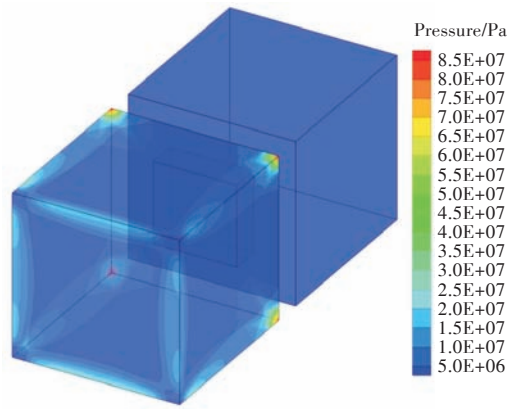

(b) t = 0.300 6 ms

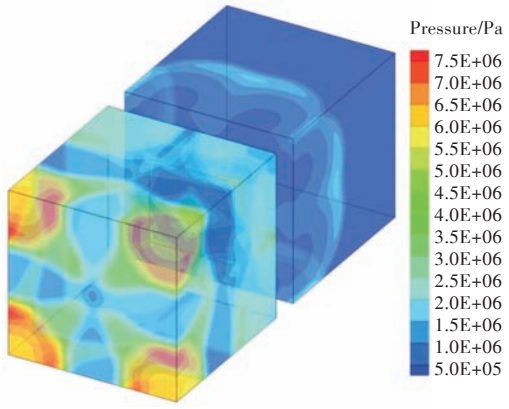

(c) t = 0.405 5 ms

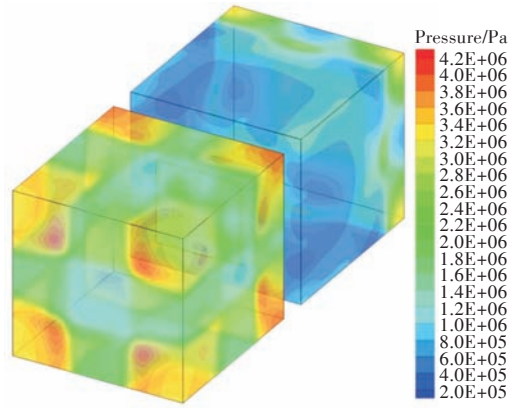

(d) t = 1.108 1 ms

Fig.17 Pressure distribution at early stage in connected space

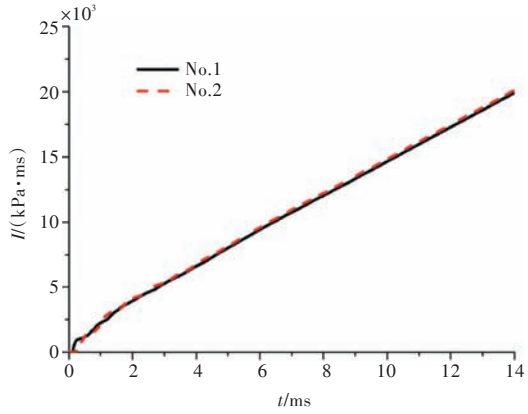

(b) Impulse time history

Fig.18 Time histories of blast load at gauging point 1 and 2 in the left confined space

points on the explosion walls in the left confined space (explosive space). As can be seen from Fig. 18, the blast load characteristics in the left confined space are similar to those in the closed space in Section 3.3. There are basically the same quasi-static overpressure peaks and impulse time histories for different measuring points.

Fig. 19 respectively shows the overpressure and impulse time histories of Nos. 3 and 4 measuring points on the explosion walls in the right confined space (space admissible for blast). As can be seen from Fig. 19, the blast load in the right confined space has the same characteristic with that in closed space of Section 3.3. The quasi-static overpressure peaks are basically the same at different measuring points and there are some differences of the impulse time histories at different measuring points.

Fig. 20 shows the overpressure and impulse time histories curves of all measuring points on the explosion walls in the connected space. It can be seen from Fig. 20(a) that the overpressure peaks of the blast waves are different in the early stage of explosion at the different measuring points of the walls, while the quasi-static overpressure peaks are basically the same (see the green heavy line in Fig. 20 (a)), which indicates that the quasi-static overpressure peak formed by the explosion in the connected space is even spatially. The feature is similar to that of the explosion in closed space. However, there is a large difference in the impulse time histories of different measuring points. The impulse of the internal measuring points in the left confined space is obviously higher than that in the right confined space (see Fig. 20(b)). The analysis shows that this is mainly because the explosion occurs in the left confined space where more energy is concentrated.

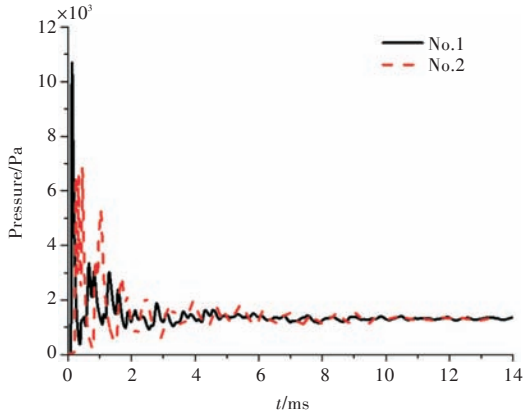

(a) Overpressure time history

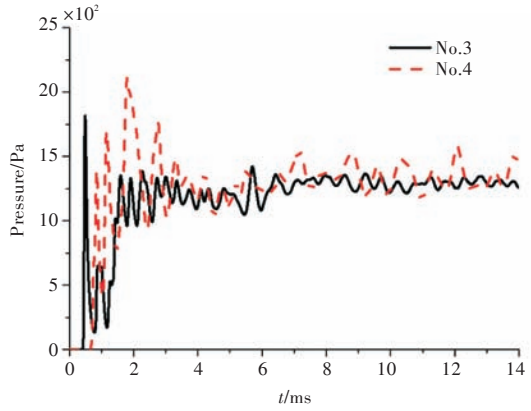

(a) Overpressure time history

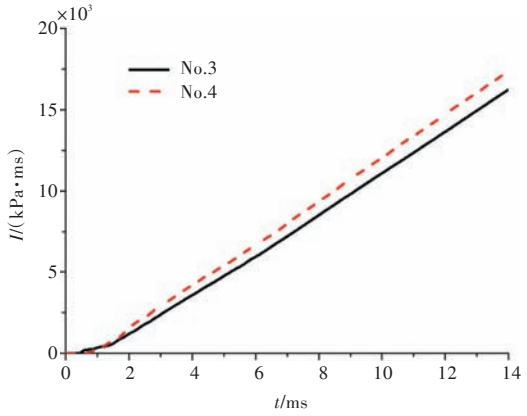

(b) Impulse time history

Fig.19 Time histories of blast load at gauging point 3, 4 in the right confined space

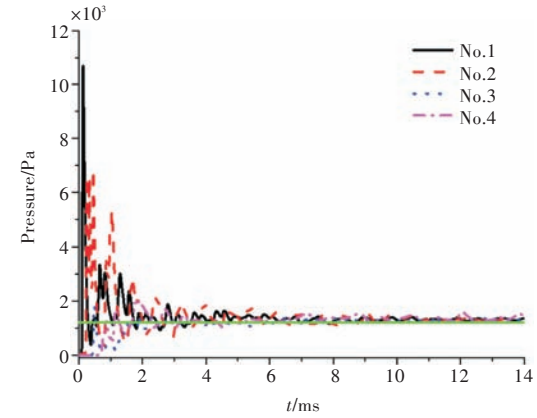

(a) Overpressure time history

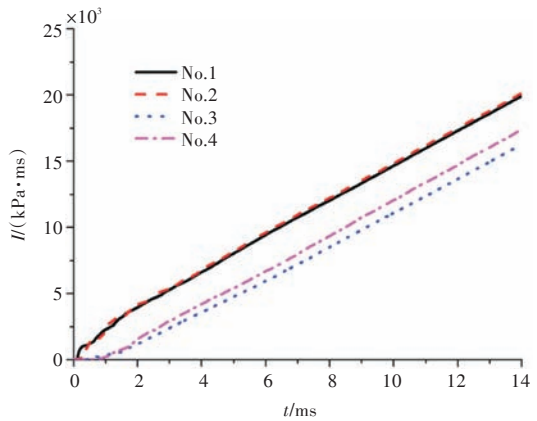

(b) Impulse time history

Fig.20 Time histories of blast load at the gauging points in connected space

6 Conclusions

Based on FORTRAN platform, this paper uses the third-order WENO finite difference scheme to independently develop an in-house high-resolution hydrocode in confined space, carries out numerical calculation of blast waves in closed, venting and connected space, and analyzes the propagation process and blast load characteristics of blast wave in confined space. Through the research, the conclusions are as follows:

1) The impulse time history curve in closed space appears to be a straight line while that in venting space appears to be a parabola.

2) The location of venting hole has little effect on the quasi-static overpressure load in venting space, but has a certain effect on the impulse time history. Shortening the relative distance between the venting hole and the explosive can reduce the impulse. The size of the venting hole has significant impacts on the blast load in the venting space. Increasing the size of venting hole can significantly accelerate the decay of quasi-static overpressure and decrease the impulse.

3) The locations of the measuring points have little effect on the quasi-static overpressure load in connected space, but have significant effect on the impulse time histories. The internal impulse of the confined space where the explosive is located is significantly higher than the internal impulse of the space into which the blast waves vent.

References

[1] ESPARZA E D, BAKER W E, OLDHAM G A. Blast pressures inside and outside suppressive structures: ADA025504 [R]. San Antonio, TX: Southwest Research Institute, 1975.

[2] KEENAN W A, TANCRETO J E. Blast environment from fully and partially vented explosions in cubicles: ADA019026[R]. [S.l.]: Department of the Army Picatinny Arsenal, 1975.

[3] EDRI I, SAVIR Z, FELDGUN V R, et al. On blast pressure analysis due to a partially confined explosion: I. Experimental studies [J]. International Journal of Protective Structures, 2011, 2(1): 1-20.

[4] WU C Q, LUKASZEWICZ M, SCHEBELLA K, et al. Experimental and numerical investigation of confined explosion in a blast chamber[J]. Journal of Loss Prevention in the Process Industries, 2013, 26(4): 737-750.

[5] HU Y, ZHU J F, ZHU K. Experimental study on explosion effect in a closed single rectangular cavity[J]. Explosion and Shock Waves, 2016, 36(3): 340-346 (in Chinese).

[6] HOU H L, ZHU X, LI W, et al. Experimental studies on characteristics of blast loading when exploded inside ship cabin[J]. Journal of Ship Mechanics, 2010, 14(8): 901-907 (in Chinese).

[7] KONG X S, WU W G, LI J, et al. Experimental research of influence of corner structure on blast loading under inner explosion [J]. Shipbuilding of China, 2012, 53(3): 40-50 (in Chinese).

[8] HOU H L, ZHU X, MEI Z Y. Study on the blast load and failure mode of ship structure subject to internal explosion[J]. Explosion and Shock Waves, 2007, 27

(2): 151-158 (in Chinese).
[9] KONG X S, WU W G, LI X B, et al. Numerical simulation of cabin structure under inner explosion[J]. Chinese Journal of Ship Research, 2009, 4(4): 7-11 (in Chinese).
[10] DING Y, CHEN Y, SHI Y C. Simplified model of overpressure loading caused by internal blast[J]. Engineering Mechanics, 2015, 32(3): 119-125, 133 (in Chinese).
[11] FAN Z Q, WANG W L, HUANG X F, et al. Simulation analysis on typical cabin internal explosion[J]. Engineering Blasting, 2015, 21(3): 13-17 (in Chinese).
[12] LIU X D, OSHER S, CHAN T. Weighted essentially non-oscillatory schemes[J]. Journal of Computational Physics, 1994, 115(1): 200-212.
[13] JIANG G S, SHU C W. Efficient implementation of weighted ENO schemes[J]. Journal of Computational Physics, 1996, 126(1): 202-228.
[14] SHU C W. Essentially non-oscillatory and weighted essentially non-oscillatory schemes for hyperbolic conservation laws[M]//QUARTERONI A. Advanced numerical approximation of nonlinear hyperbolic equations. Berlin Heidelberg: Springer, 1998: 325-432.
[15] SHU C W. High order weighted essentially nonoscillatory schemes for convection dominated problems[J]. Siam Review, 2009, 51(1): 82-126.
[16] HARTEN A, ENGQUIST B, OSHER S, et al. Uniformly high order accurate essentially non-oscillatory schemes, III[J]. Journal of Computational Physics, 1987, 71(2): 231-303.
[17] CAO L. Three-dimensional computations on capturing of gas-water interface by level set method[D]. Hefei: University of Science and Technology of China, 2009 (in Chinese).
[18] XIE C T. The study on R-M instability of the material interface in gas-water compressible flow[D]. Harbin: Harbin Engineering University, 2011 (in Chinese).
[19] SHU C W, OSHER S. Efficient implementation of essentially non-oscillatory shock-capturing schemes[J]. Journal of Computational Physics, 1988, 77(2): 439-471.
[20] SOD G A. A survey of several finite difference methods for systems of nonlinear hyperbolic conservation laws[J]. Journal of Computational Physics, 1978, 27(1): 1-31.
[21] WOODWARD P, COLELLA P. The numerical simulation of two-dimensional fluid flow with strong shocks[J]. Journal of Computational Physics, 1984, 54(1): 115-173.
[22] ANDERSON C E Jr, BAKER W E, WAUTERS D K, et al. Quasi-static pressure, duration, and impulse for explosions (e.g. HE) in structures[J]. International Journal of Mechanical Sciences, 1983, 25(6): 455-464.

爆炸波高精度数值计算程序开发及应用

徐维铮[1,2], 吴卫国[1,2]
1 武汉理工大学 高性能舰船技术教育部重点实验室,湖北 武汉 430063
2 武汉理工大学 交通学院,湖北 武汉 430063

摘　要:[**目的**]当爆炸发生在约束空间内部,由于壁面的约束限制,爆炸冲击波的传播和演化特性将更加复杂,其对结构、内部设施及人员的损伤也更加严重。为了研究约束空间内部的爆炸特性,[**方法**]基于FORTRAN平台,采用三阶WENO有限差分格式,自主开发约束空间内部爆炸波高精度三维数值计算程序。利用Sod激波管、双爆轰波碰撞、空中爆炸等经典算例,验证所开发程序的可靠性。基于验证的程序,开展约束空间内部爆炸波数值计算,研究密闭空间、泄压空间及连通空间内部的爆炸波传播规律与爆炸载荷特性。[**结果**]研究表明,所开发的程序能较好地模拟约束空间内的爆炸过程。[**结论**]该开发工作可为后续研究复杂空间内部爆炸波传播路径、评估爆炸载荷以及合理设计抗爆结构奠定基础。

关键词:爆炸冲击波;约束空间;数值模拟;高精度计算程序;WENO格式;程序开发